Two-Dimensional Infrared Femtosecond Spectroscopy of Cyclic Pentapeptides [1]

Andrei Piryatinski, Vladimir Chernyak and Shaul Mukamel

Department of Chemistry, University of Rochester
Rochester, N. Y. 14627

Abstract. The multidimensional optical response of the amide I band of the pentapeptide (cyclo(D-Abu-Arg-Gly-Asp-Mamb)) is computed using the vibrational-exciton model, treating each peptide unit as a localized anharmonic vibration. The absolute value, the real and the imaginary parts of the 2D photon echo signal are simulated by solving the nonlinear exciton equations (NEE). The signatures of the one- and two-vibrational-exciton dynamics associated with different models of spectral broadening (homogeneous as well as diagonal and off-diagonal static disorder) are discussed.

INTRODUCTION

The infrared absorption of proteins and polypeptides in the amide I (1600-1700 cm^{-1}) spectral region originates from the stretching motion of the peptide CO bond. This mode has a strong ($\sim$ 0.4 D) transition dipole moment and is clearly distinguishable from other vibrational modes of the amino-acid side chains. Early study of symmetric model-polypeptides conducted by Krimm and Bandeker, have demonstrated that the dipole-dipole interaction between the CO stretching modes results in the delocalization of amide I states [1], which can be modeled as Frenkel vibrational excitons. Assuming dipole-dipole coupling between peptide groups, Torii and Tasumi, performed computer simulations of the absorption lineshape for a few mid-size ($\sim$ 100 peptide) globular proteins with known structures, and obtained good agreement with experiment [2]. The dependence of the coupling on relative orientations and distances of the interacting dipoles results in a unique amide I band signature of the particular secondary structure motif. This is widely utilized in studying protein and polypeptide structures [3,4].

The information extracted from ordinary one-dimensional (1D) IR spectra is limited since the amide I band consists of a number of unresolved spectral lines associated with vibrational motions of different structural elements. Conformational fluctuations within a particular three-dimensional protein structure, and lo-

[1)] Submitted to the Proceedings of International Symposium on Two-Dimensional Correlation Spectroscopy, Y. Ozaki, Ed.

cal interaction with solvent induce inhomogeneous broadening, and the spectrum is typically highly congested. Multidimensional visible and infrared techniques offer a broad range of novel spectroscopies which can probe the structure and dynamics of complex molecules, aggregates, solvent-solute interactions and molecular liquids. A variety of multidimensional off-resonant Raman [5–9] and resonant optical and IR techniques have been developed [10–14].

In this paper we discuss the structure of the one- and two-exciton manifold of pentapeptides and how it may be probed using 2D IR techniques. Signatures of the one- and two-exciton dynamics are discussed for different models of line broadening. In resonant infrared multidimensional spectroscopies the excitation pulses couple directly to the transition dipoles. The lowest order possible techniques in noncentrosymmetric media involve three-pulses (see Fig. 1 (A)). Simulating the signal requires calculation of the third order response function. Since the third order response of coupled anharmonic vibrations (Fig. 1 (B)) depends on the complete set of one- and two-exciton states (Fig. 1 (C)) coupled to thermal bath [14], the direct sum-over-states computation is prohibitively expensive for large molecules.

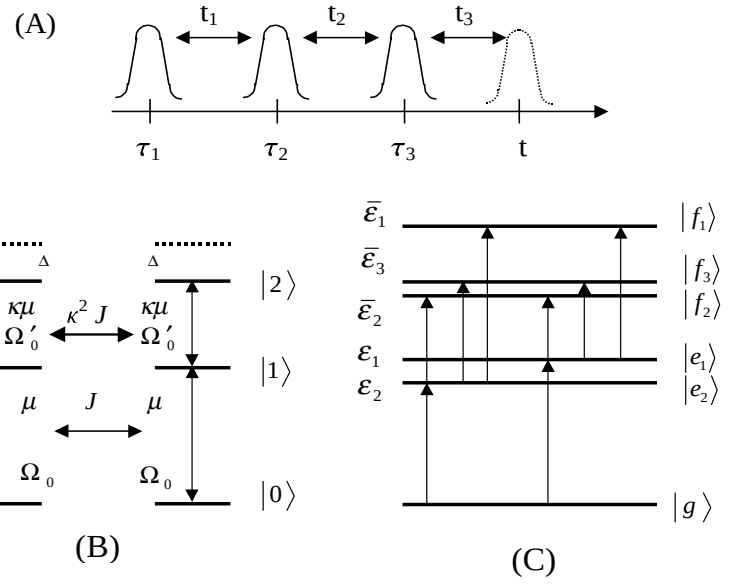

FIGURE 1. (A) Pulse sequence in three-pulse experiment. (B) Peptide units modeled as anharmonic vibrations with $0-1$ transition energy Ω_0 and $1-2$ transition energy Ω_0', and anharmonicity $\Delta = \Omega_0' - \Omega_0$. Coupling energy between the vibrations is J and κJ. $0-1$ transition dipole is μ and $1-2$ transition dipole is $\mu' = \kappa\mu$. (C) Exciton states. Arrows show all possible transitions to one-exciton manifold $\{|e_1>, |e_2>, \ldots, |e_5>\}$, and between one and two-exciton $\{|f_1>, |f_2>, |f_3>, \ldots, |f_{15}>\}$) manifolds.

An alternative quasiparticle description of the optical response is possible using the nonlinear exciton equations (NEE) [15]. The response function is expressed in terms of one-exciton Green functions and the exciton-exciton scattering matrix. Four coherent ultrafast 2D techniques have been proposed [12,13]. We shall focus on

2D photon echo (PE) spectroscopy whereby the system first interacts with a single femtosecond pulse with wavevector $\mathbf{k_1}$, and then simultaneously ($t_2 = 0$) with a pair of pulses having $\mathbf{k_2}$ and $\mathbf{k_3}$ wavevectors and delayed by the time t_1. By mixing the third order signal with a gating pulse with delay time t_3, the heterodyne signal can be measured in the direction determined by the phase matching conditions $\mathbf{k_s} = \mathbf{k_3} + \mathbf{k_2} - \mathbf{k_1}$. We shall display the 2D PE signal in the frequency-domain by performing a double Fourier transform

$$S(\Omega_2, \Omega_1) = \int_0^\infty dt_3 \int_0^\infty dt_1 \exp(i\Omega_2 t_3 + i\Omega_1 t_1) S(t_3, 0, t_1). \quad (1)$$

Experimental 2D IR PE study of stretching motion of carbon monoxide in myoglobin-CO and rare-earth carbonyls were carried out by Fayer and coworkers [10]. Femtosecond pump-probe and dynamic hole burning 2D IR studies of the amide I spectral region of several small proteins has been reported by Hamm, Lim, and Hochstrasser [11]. Similar to 2D NMR spectroscopy, the sensitivity of the 2D IR signal to protein geometry can be used for structure determination, as demonstrated by pump-probe and dynamic hole burning measurements on a model pentapeptide *cyclo*-Abu-Arg-Gly-Asp-Mamb [16]. Computer simulations of the 2D IR PE signal from glycine dipeptide and cyclic pentapeptide, based on the NEE approach were carried out [17,18].

VIBRATIONAL-EXCITON MODEL

The atomic coordinates of the pentapeptide used in our study are known from its crystallographic structure [19], shown in Fig. 2. We model each CO bond as a three level system (Fig. 1 (B)). The dipole-dipole couplings among CO vibrations

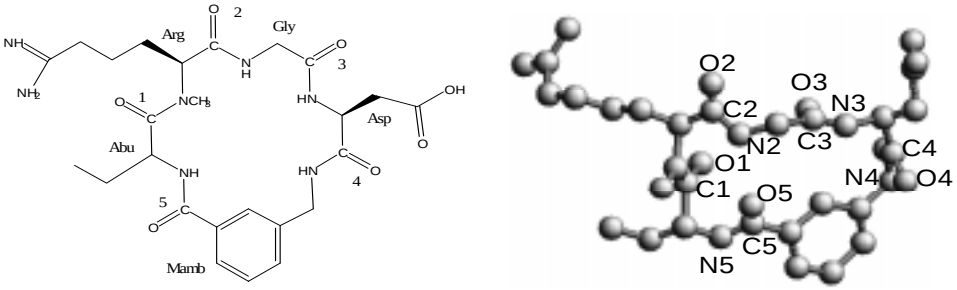

FIGURE 2. 3D structure of the pentapeptide [19].

were calculated by assigning each dipole on a CO bond 0.868 $\mathring{A}$ from carbon atom and forming 25° angle of with respect to the bond. The absolute value of each dipole moment is $0.37D$. [1,2,11,16]. The central frequencies for the peptide CO vibrations are adopted from Ref. [16]. Using these parameters, the one-exciton Hamiltonian (in cm^{-1}) is

$$h = \begin{pmatrix} 1588 & 7.2 & 5.7 & -1.7 & -7.0 \\ 7.2 & 1671 & -0.7 & 0.6 & -7.6 \\ 5.7 & -0.7 & 1648 & 2.2 & -6.2 \\ -1.7 & 0.6 & 2.2 & 1610 & 0.3 \\ -7.0 & -7.6 & -6.2 & 0.3 & 1618 \end{pmatrix} \quad (2)$$

where the matrix element indices are related to the peptide group numbers shown in Fig. 2. Since the difference between the absolute values of the central frequencies in Eq. (2) is larger that the coupling energies, each one-exciton state is a weakly-perturbed localized CO vibration. The eigenfrequencies of the Hamiltonian Eq. (2) are $\varepsilon_1 = 1586cm^{-1}$, $\varepsilon_2 = 1610cm^{-1}$, $\varepsilon_3 = 1617cm^{-1}$, $\varepsilon_4 = 1650cm^{-1}$, and $\varepsilon_5 = 1673cm^{-1}$.

The two-exciton manifold is formed by two types of doubly-excited vibrational states. The first are overtone two-excitations (OTE) where a single bond is doubly excited, and the other are collective two-excitations (CTE) where two-bonds are simultaneously excited [17,20]. A pentapeptide has 5 OTE and 10 CTE. The fifteen two-exciton energies are obtained from the poles of the exciton scattering matrix [20,15,13], by assuming that the ratio of the $1-2$ to $0-1$ transition dipole moments of a single peptide unit is $\kappa = \sqrt{2}$ for all peptides, as well as the anharmonicities are equal for all peptides and set to $\Delta = -16cm^{-1}$ according to the experiment [11,16]. The two-exciton state eigenenergies are $\bar{\varepsilon}_1 = 3157cm^{-1}$, $\bar{\varepsilon}_2 = 3195cm^{-1}$, $\bar{\varepsilon}_3 = 3200cm^{-1}$, $\bar{\varepsilon}_4 = 3205cm^{-1}$, $\bar{\varepsilon}_5 = 3220cm^{-1}$, $\bar{\varepsilon}_6 = 3227cm^{-1}$, $\bar{\varepsilon}_7 = 3235cm^{-1}$, $\bar{\varepsilon}_8 = 3258cm^{-1}$, $\bar{\varepsilon}_9 = 3259cm^{-1}$, $\bar{\varepsilon}_{10} = 3264cm^{-1}$, $\bar{\varepsilon}_{11} = 3283cm^{-1}$, $\bar{\varepsilon}_{12} = 3287cm^{-1}$, $\bar{\varepsilon}_{13} = 3288cm^{-1}$, $\bar{\varepsilon}_{14} = 3322cm^{-1}$, and $\bar{\varepsilon}_{15} = 3331cm^{-1}$. In general the two-exciton eigenstates are linear combinations of the OTE and the CTE. However, for the present pentapeptide, most two-exciton states can be classified as weakly perturbed OTE or STE type.

To explore the signatures of homogeneous and inhomogeneous broadening in 2D PE spectra, we consider different line-broadening models. We denote the dephasing rate of the first vibrational transition and the overtone by Γ and $\gamma^{(2)}$, respectively. In all calculations Γ and $\gamma^{(2)}$ are set identical for all peptide groups. Anharmonicity Δ is fixed and independent on disorder. We have employed the following six models:

(A) Small homogeneous dephasing rates: $\Gamma = 0.2cm^{-1}$, and $\gamma^{(2)} = 0.4cm^{-1}$.

(B) Large homogeneous dephasing rates: $\Gamma = 5cm^{-1}$, and $\gamma^{(2)} = 10cm^{-1}$, which correspond typical to experimental values [11,16].

(C) Uncorrelated static diagonal disorder with variance $\sigma_d = 12cm^{-1}$ equal for all peptide groups. $\Gamma = 0.2cm^{-1}$, $\gamma^{(2)} = 0.4cm^{-1}$.

(D) Same as model (C) except that the homogeneous dephasing rates of each peptide are adopted from experiment and set to $\Gamma = 5cm^{-1}$, $\gamma^{(2)} = 10cm^{-1}$.

(E) Uncorrelated static off-diagonal disorder with variances $\sigma_{od} = 12cm^{-1}$ equal for all peptide groups. The homogeneous dephasing rates are $\Gamma = 0.2cm^{-1}$, $\gamma^{(2)} = 0.4cm^{-1}$.

(F) Same as model (E) except that the homogeneous dephasing rates are taken from experiment and set to $\Gamma = 5cm^{-1}$, $\gamma^{(2)} = 10cm^{-1}$.

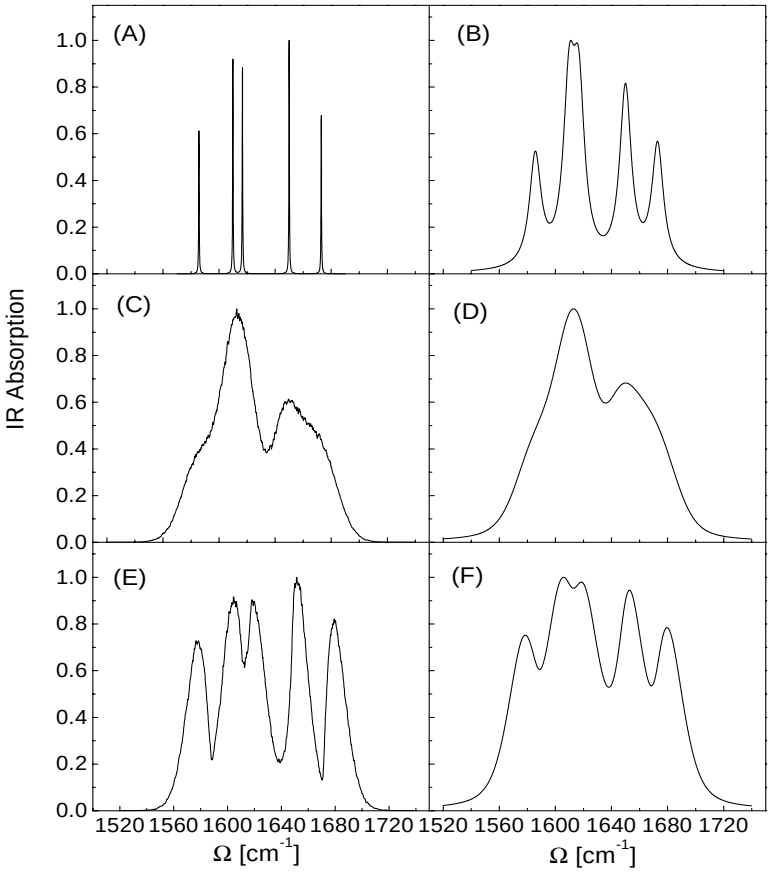

FIGURE 3. Infrared absorption (1D) spectra for models (A)-(F).

The linear (1D) absorption spectra of all models are presented in Fig. 3. Model (A) shows five well-resolved one-exciton lines. In model (B) the lines ε_2 and ε_3 are poorly resolved due to the increased homogeneous broadening. Diagonal disorder in models (C) and (D) further broadens the spectra. Since off-diagonal disorder induces state delocalization, the one-exciton resonances shift for models (E) and (F) and become $\varepsilon_1^{'} = 1578cm^{-1}$, $\varepsilon_2^{'} = 1605cm^{-1}$, $\varepsilon_3^{'} = 1618cm^{-1}$, $\varepsilon_4^{'} = 1652cm^{-1}$, and $\varepsilon_5^{'} = 1679cm^{-1}$.

ABSOLUTE VALUE, REAL AND IMAGINARY PARTS OF 2D PHOTON ECHOES

Calculations of 2D PE heterodyne signal $S(\Omega_2, \Omega_1)$ were performed using Eqs. (E1) and (E2) of Ref. [13]. Numerical work involved the calculation of the exciton-exciton scattering matrix, following the procedure described in Appendix A of Ref. [13], and evaluating the integral in Eq. (E2) [13]. The 2D PE signal for models (C) - (F) was averaged over 10^5 disorder realizations.

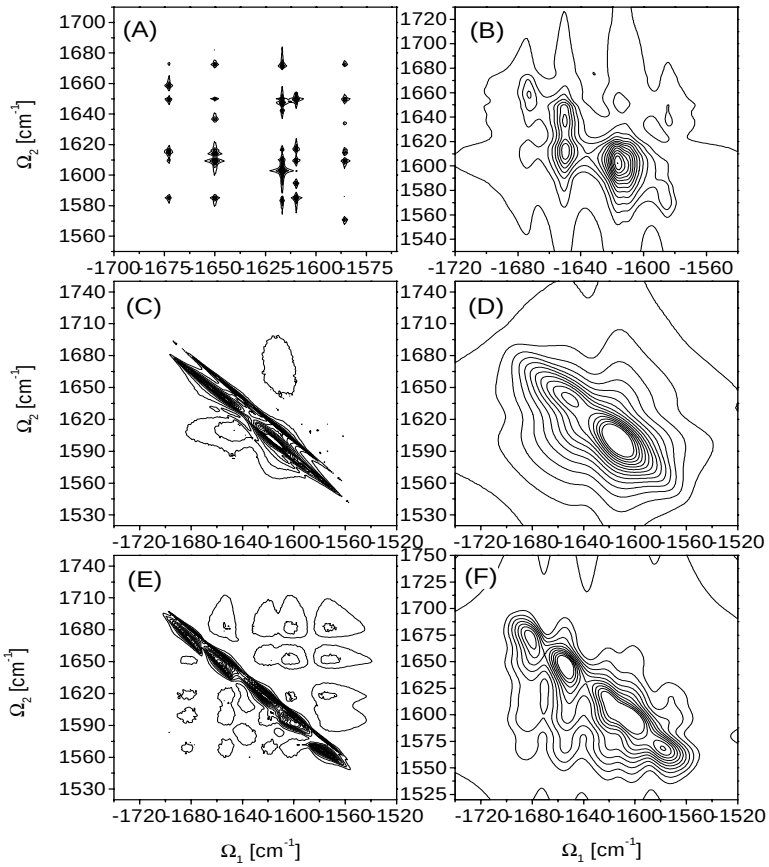

FIGURE 4. Absolute value $|S(\Omega_2, \Omega_1)|$ of 2D infrared photon echo signal for models (A)-(F).

Figure 4 shows the calculated absolute value of 2D PE signal $|S(\Omega_2, \Omega_1)|$. The resonances representing various correlations between one-exciton states $(-\varepsilon_a, \varepsilon_a)$ (diagonal peaks) and $(-\varepsilon_a, \varepsilon_b)$ $a \neq b$ and $a, b = 1, \ldots, 5$ (off-diagonal peaks) as well as between one- and two-exciton states $(-\varepsilon_a, \bar{\varepsilon}_b - \varepsilon_a)$, $a, b = 1, \ldots, 5$ (cross-peaks), are well resolved in model (A). Model (B) has the same resonant energies, however since homogeneous broadening is comparable with the anharmonicity and coupling energies, many resonances are unresolved. Slices of the 2D spectra along the Ω_2 direction at $\Omega_1 = -\varepsilon_2$, for models (A) and (B) are displayed in Fig. 5.

The 2D PE signal for models (C) and (D), displayed in Fig. 4 shows inhomogeneously broadened resonances stretched along the $-\Omega_1 = \Omega_2$ direction. They represent self-correlations of the one-exciton states and correlations between one-exciton and two-exciton (OTE) states on the same sites. The other resonances make a negligible contribution to these spectra due to the uncorrelated disorder distribution. Slices of the 2D signal of models (C) and (D) along Ω_2 at $\Omega_1 = -\varepsilon_2$ are shown in Fig. 5. The slice of model (C) contains two distinct peaks. The narrow one (width Γ) represents self-correlation of the one-exciton states and the broader one (width $\gamma^{(2)} + \Gamma$) is due to the OTE state. The energy splitting between the

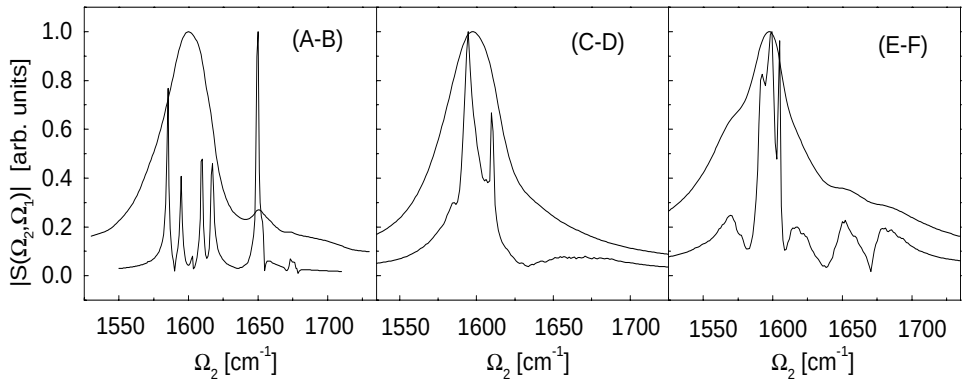

FIGURE 5. Slices of the signals of Fig. 4 for models (A) - (D) at $\Omega_1 = -\varepsilon_2$ and for models (E)-(F) at $\Omega_1 = -\varepsilon_2'$ Model (A), (C), (E) show detailed structure, the broader curves correspond to model (B), (D), and (F).

maxima provide with the exciton state anharmonicity close to Δ.

The 2D PE signal (Fig. 4) of models (E) and (F) is dominated by inhomogeneous broadening along the $-\Omega_1 = \Omega_2$ direction of the diagonal peaks and the cross-peaks associated with the OTE states. In addition, weak off-diagonal and the cross-peaks are clearly seen in the plot. Slice of the 2D PE signal along Ω_2 at $\Omega_1 = -\varepsilon_2^{'}$, are shown in Fig. 5. In contrast to models (C) and (D), energy differences between the maxima of the one-exciton and strong two-exciton resonances are not equal to Δ, indicating that the relevant two-exciton states are not necessarily localized (OTE type).

The real and imaginary parts of the PE signal for models (B), (D), and (F) are displayed in Fig. 6. Slices of this 2D signal are shown in Fig. 7. According to this plot, in the vicinity of the resonances, the real part of the signal (dotted lines) is dispersive, while the imaginary part (solid line) has a negative minimum. Analysis of the sign variation of the real and imaginary parts in different directions [18] indicates that for close disorder realizations the resonances should add up constructively in the directions $-\Omega_1 \sim \Omega_2$, and destructively in the perpendicular direction.

CONCLUSIONS

We have applied the vibrational exciton model to describe the infrared response of a cyclic pentapeptide in the amide I spectral region. The 2D PE signal has been calculated by solving the NEE. The one- and two-exciton states of the pentapeptide are well localized. Different models of homogeneous and inhomogeneous line broadening show distinct 2D patterns. All resolved resonances associated with one-exciton correlations (diagonal and off-diagonal peaks) as well as those associated with one- and two-exciton state correlations (cross-peaks) in models (A)-(B) are identified from the absolute value of the signal. Uncorrelated diagonal disorder

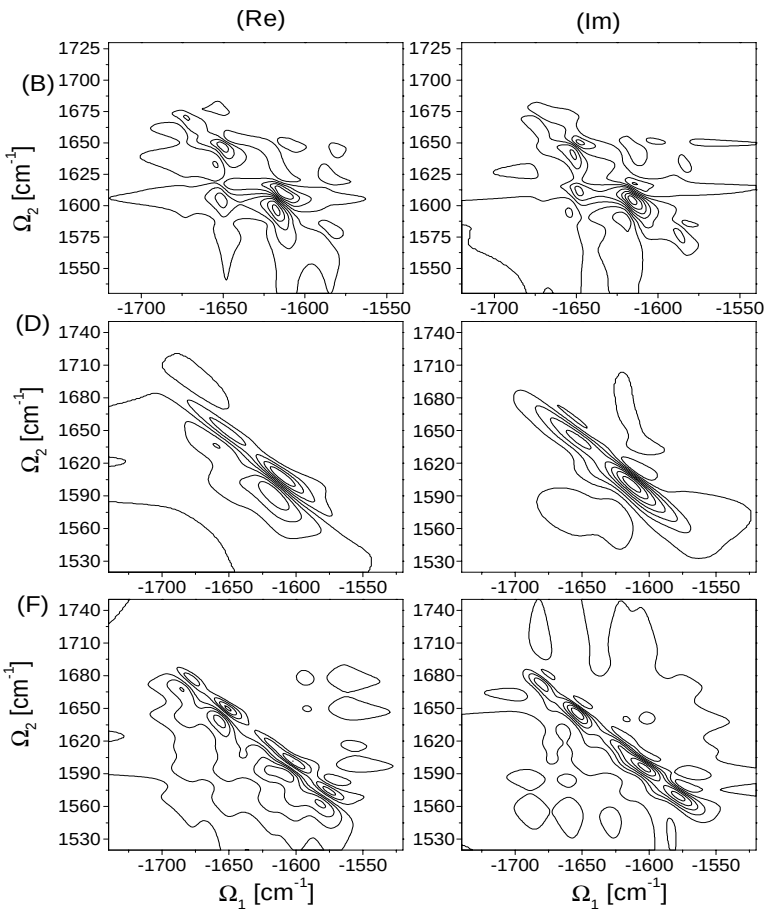

FIGURE 6. Real and imaginary parts of 2D signal $S(\Omega_2, \Omega_1)$ for models (B), (D), and (F) (large homogeneous dephasing).

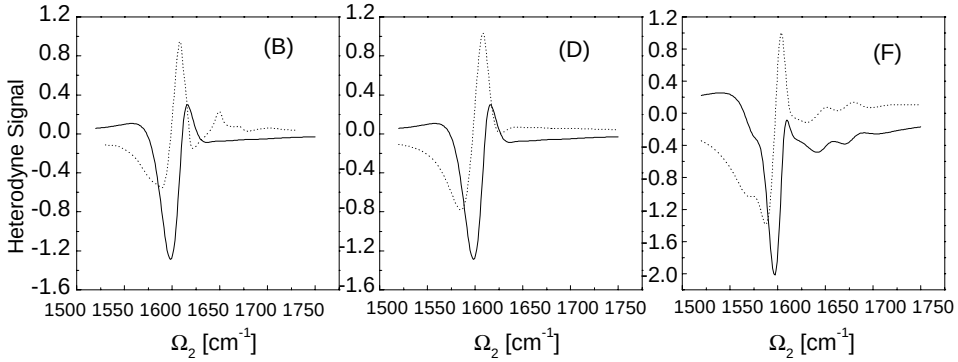

FIGURE 7. Slices of the signals of Fig. 6 for models (B), (D) at $\Omega_1 = -\varepsilon_2$ and for model (F) at $\Omega_1 = -\varepsilon_2'$. Dotted (solid) line is real (imaginary) part of the heterodyne signal.

[models (C) and (D)] induces inhomogeneous broadening of the 2D PE spectra along $-\Omega_1 = \Omega_2$ directions. In this case the signal has diagonal peaks (due to one-exciton self correlations) and cross-peaks due to correlations of the one-exciton states with the OTE excited on the same peptide group. Off-diagonal disorder [models (E) and (F)] induces exciton delocalization over two peptides. In this case the signal contains inhomogeneously broadened diagonal, off-diagonal, and cross-peaks. Examination of the real and the imaginary parts of the 2D PE signal shows that in the vicinity of the 2D resonances, its profile is determined by the the ratio of the real and the imaginary parts of the exciton scattering matrix. Static disorder may lead to the formation or the destruction of echoes in various directions.

ACKNOWLEDGEMENTS

We gratefully acknowledge the support of the National Science Foundation and the United States Air Force Office of Scientific Research.

REFERENCES

1. S. Krimm and J. Bandeker, *J. Adv. Protein Chem.*, **38**, 181, (1986).
2. H. Torii and M. Tasumi, *J. Chem. Phys.*, **96**, 3379, (1992).
3. W. K. Surewicz and H. H. Mantsch,*Biochem. Biophys. Acta*, **952**, 115, (1988). W. K. Surewicz, H. H. Mantch, and D. Chapman, *Biochemistry*, **32**, 389, (1993). M. Jeckson, H. Mantsch, *Crit. Rev. Biochem. Mol. Biol.*, **30**, 95, (1995).
4. R. B. Dyer, F. Gai, W. H. Woodruff, R. Gilmanshin, R. H. Callender, *Acc. Chem. Res.*, **31**, 709, (1998).
5. Y. Tanimura and S. Mukamel, *J. Chem. Phys.* **99**, 9496 (1993). V. Khidekel and S. Mukamel, *Chem. Phys. Lett.* **240**, 304 (1995).
6. V. Chernyak and S. Mukamel, *J. Chem. Phys.* **108**, 5812, (1998).
7. A. Piryatinski, V. Chernyak, and S. Mukamel, in *Ultrafast Phenomena XI*, edited by T. Elsaesser, J. G. Fujimoto, D. A. Wiersma, W. Zinth, (Springer, 1998), p.541; S. Mukamel, A. Piryatinski, and V. Chernyak, *J. Chem. Phys.*, **110**, 1711, (1999).
8. V. Chernyak, A. Piryatinski, and S. Mukamel, *Laser Chem.*, **19**, 109, (1999).
9. S. Mukamel, A. Piryatinski, and V. Chernyak, *Acc. Chem. Res.*, **32**, 145, (1999).
10. K. D. Rector, A. S. Kwok, C. Ferrante, A. Tokmakoff, C. W. Rella, and M. D. Fayer, *J. Chem. Phys.*, **106**, 10027, (1997).
11. P. Hamm, M. Lim, and R. M. Hochstrasser, *J. Phys. Chem. B*, **102**, 6123, (1998).
12. W. M. Zhang, V. Chernyak, and S. Mukamel, in *Ultrafast Phenomena XI*, edited by T. Elsaesser, J. G. Fujimoto, D. A. Wiersma, W. Zinth, (Springer, 1998), p. 663; S. Mukamel, W. M. Zhang, and V. Chernyak, in *Photosynthesis: Mechanisms and Effects*, G. Garab Ed., (Kluwer, Dordrecht), **1**, 3 (1998).
13. W. M. Zhang, V. Chernyak, and S. Mukamel, *J. Chem. Phys.*, **110**, 5011, (1999).
14. S. Mukamel, *Principles of Nonlinear Optical Spectroscopy*, (Oxford University Press, New York, (1995)).

15. V. Chernyak, W. M. Zhang, and S. Mukamel, *J. Chem. Phys.*, **109**, 9587, (1998).
16. P. Hamm, M. Lim, W. F. DeGrado, and R. Hochstrasser, *Proc. Nat. Acad. Sci.*, **96**, 2036, (1999).
17. A. Piryatinski, S. Tretiak, V. Chernyak, and S. Mukamel, *J. Raman Spectrosc.*, (in press).
18. A. Piryatinski, V. Chernyak, and S. Mukamel, in *Ultrafast Infrared and Raman Spectroscopy*, M. D. Fayer Ed. (Marcel Dekker, New York), (in press).
19. A. C. Bach, C. J. Eyermann, J. D. Gross, M. J. Bower, R. L. Harlow, P. C. Weber, and W. F. DeGrado, *J. Am. Chem. Soc.*, **116**, 3207, (1994).
20. O. Kühn, V. Chernyak, and S. Mukamel, *J. Chem. Phys.*, **105**, 8586, (1996).